Development and Analysis of a Nested Multiscale Model of Hepatitis B Viral Infection

O. T. Ogunfowote [1,2]

1. Modeling Health and Environmental Linkages Research Group (MHELRG),
2. Department of Mathematical and Computational Sciences, University of Venda, South Africa.
Corresponding author: toydel2013@gmail.com, ogunfowoteot@tasued.edu.ng

Abstract

Hepatitis B remains a global health concern owing to its deadly nature. A Nested Multiscale Model was developed by applying the Replication-Transmission Theory at the cell level of biological organisation. A new set of measures to assess infectiousness at the individual and community levels was presented at the biological organisation's cell level, where we grounded our analysis. These models make it possible to investigate the dynamics of the virus within infected cells, as well as the dynamics of future cell infections and the discharge of the virus from infected cells. To study quantitatively how the dynamics of within-cell replication affect the dynamics of between-cell transmission, mathematical analysis and numerical simulations were carried out. These simulations can be used to evaluate the effectiveness of treatment and preventive interventions.

1   Introduction

An infectious disease system is a complex system that consists of three main interacting subsystem which are the environmental sub-system, the pathogen sub-system and the host sub-system. The complex nature of infectious disease system makes their aggregate dynamics nonlinear. They continue to debilitate and to cause death in humans and animals, with new disease-causing pathogens

emerging and old pathogens reemerging or evolving [1]. An infectious disease system is organised into seven primary levels. Developing efficient preventive and control strategies against endemics and improving our understanding of disease dynamics have both benefited greatly from mathematical modeling of infectious diseases [2]. Several mathematical models have examined different facets of Hepatitis B and the immunological response that occurs during infection. It should come as no surprise that the host immune responses to HBV infection are also incredibly complex in their natural history [3]. Mathematical models of HBV studied in the past have revealed virus production levels, virus clearance rates, half-life of infected cells, but was unable to aid the development of successful HBV drug treatments as a result of ignoring the spatial aspect of infection [4]. Multiscale modeling have improved the treatment of viral infections through the introduction of Direct-Acting Antiviral Agents (DAAs). In the case of anti-HCV medications, DAAs with various antiviral mechanisms have significantly increased the infected host's sustained virological response (SVR) rate; nevertheless, they also come with emerging resistance and are not effective against all genotypes. To prevent the emergence of medication resistance, care must be taken in determining an efficient treatment plan.

Millions of individuals worldwide are impacted by the major public health issue of the hepatitis B virus (HBV). Hepatocytes are the parenchymal cells of the liver that are infected with HBV, which can lead to acute or chronic illness. It belongs to the family Hepadnaviridae and is a hepatotropic noncytopathic DNA virus. The virus that infects the hepatocyte is not cytotoxic, meaning it spreads without destroying the host cell. HBV can be spread vertically, parenterally (from an infected mother to a kid, leading in a second infection that becomes chronic in 90% of cases), sexually, or by blood-borne contact such as blood transfusions or intervening drug usage. [5]. When a virion binds to a cell surface receptor, the virus's life cycle begins. The nucleocapsid then enters the cytoplasm and is released. After being delivered to a nuclear pore, the nucleocapsid breaks down and releases rcDNA into the nucleus [6]. Within the nucleus, rcDNA is repaired by the host enzymes and it is converted to covalently closed circular DNA (cccDNA) which serves as template for pregenomic RNA (pgRNA) and precore and subgenomic mRNAs, whose translation yields HBV polymerase and core proteins, hepatitis B e-antigen (HbeAg), and SML-HBsAg respectively [6, 7]. HBV polymerase and pgRNA are bundled into freshly produced capsids, where they are reverse transcribed to produce offspring rcDNA. At the endoplasmic reticulum, mature rcDNA-containing capsids are encapsulated and secreted through multivesicular structures. An alternative is to recycle these capsids into the nucleus, where they release fresh rcDNA that can restore the pool of cccDNA (intracellular recycling) [8].

Multiscale modeling is a powerful tool for studying complex systems at multiple levels of organisation. It involves the integration of models at different scales to capture and relate the behaviour of the system at different levels of organisation. Compare to conventional single-scale models (see [9, 10, 11, 12, 13, 14] and references therein), multiscale modeling offers a more thorough and accurate knowledge of complex systems. A new and improved method will be needed to research viral infection dynamics because the majority of mathematical models used to study viral infectious illnesses are single scale and unable to fully capture the complex character of viral infections. Understanding the mechanisms at the various infectious illness scales and how these scales interact is essential to comprehending the transmission of infectious disease systems in depth. Although this can be expanded to other categories, the within-host and between-host scales are the two most researched scales in the transmission of infectious disease systems. Multiscale models of infectious

disease systems can be empirical models (which characterise infectious disease system at more than one scale) or can be quantitative models (that also characterise infectious disease system at more than one scale) [15]. Multiscale modeling is applied to systems that have important features across many others of magnitude in time and space. The model facilitates the description and understanding of problem that span across several orders of spatial and temporal scales. Many modeling issues related to infectious diseases, including tuberculosis [16], influenza infections [17], hepatitis C virus [18, 19], malaria [20], influenza A virus [21, 22], and so forth, have been addressed by multiscale models.

Even though the significance of multiscale study of infectious disease dynamics has been acknowledged, the multi-spatial and/or multi-temporal scales of the disease systems have not been addressed in the vast majority of published publications so far that have concentrated on modeling infectious disease dynamics. The lack of strong foundational knowledge to support the development of multiscale modeling of infectious disease systems on three main frontiers — the conceptual framework frontiers, the scientific applications frontiers, and the mathematical technology frontiers may be partly blamed for these [23]. For the purpose of this study, the categorisation framework developed and presented in [15, 24] will be adopted. Garira's work summarises the host sub-system model into seven main levels. He suggests naming each multiscale model after the level of multiscale observation of an infectious disease system at which it is developed. This results in seven main levels of multiscale models: cell level multiscale models (cL - MSMs), tissue level multiscale models (TL - MSMs), organ level multiscale models (OL - MSMs), microecosystem level multiscale models (mL - MSMs), host level multiscale models (HL - MSMs), community level multiscale models (CL - MSMs) and macrosystem level multiscale models (ML - MSMs). There are five generic categories of multiscale models of infectious disease systems that has been developed at different levels of an infectious disease system by integrating two adjacent scales at a time and they are: (i) Individual based multiscale models (IMSMs) (ii) Nested multiscale models (NMSMs) (iii) Embedded multiscale models (EMSMs) (iv) Hybrid multiscale models (HMSMs) (v) Coupled multiscale models (CMSMs) [15]. As noted in [25], every one of the seven primary levels of organisation of an infectious disease system as a level of multiscale observation can be produced at any of the categories. It is significant to remember that the category of the multiscale model to be used will depend on the features of the problem to be studied. In multiscale modeling, the following processes are involved: transmission, shedding / excretion, superinfection, and infection.

In this study, we used Hepatitis B as a case study at the cell level to construct a nested multiscale model for hepatic viral infection based on the Replication - Transmission Relativity Theory [25]. Replication-Transmission Relativity Theory states that at any level of organisation of an infectious diseases system there is no privileged / absolute scale which would determine disease dynamics, only interactions between the microscale and macroscale identifies an infectious disease system as a complex system which is organised into seven main hierarchical levels at which host-pathogen interactions can play out [24, 25]. This theory, which takes into consideration the interplay of two scales at a level of organisation of an infectious disease system, is an extension of the Transmission Mechanism Theory. The two scales are microscale (pathogen replication) and macroscale (pathogen transmission). Multiscale models at this level of organisation are developed using the cell level as the level of multiscale observation with the (i) within - tissue scale, (ii) within - organ scale, or (iii) within - host scale as the scale of analysis. It should be noted that the multiscale models at this level is only suitable for evaluating medical interventions that operate at the within-host scale such

as drugs and vaccines. In order to create the nested multiscale model, we will upscale the individual host infectiousness (within-cell scale viral load) to population level infectiousness (community viral load).

Most of the Mathematical Models employed to study viral infectious diseases are single scales and are unable to describe the complex nature of viral infections in detail, hence a new and improved approach will be required to study viral infection dynamics. We employed slow and fast scale analysis to upscale the microscale parameters to the macroscale variables in this study, and we also made an effort to distinguish between complete virions and incomplete particles, which was not taken into consideration in the work of [26]. This allowed us to describe a nested multiscale model of Hepatitis B viral infection. The paper is organised as follows. In section 2 we developed a nested multiscale model for viral hepatitis using hepatitis B viral Infections as an example at the cell-level. We emphasise on the time mismatch which is one of the misconception to the study of multiscale modeling as a complex system. Section 3 contained the mathematical analysis of the model and the numerical simulation (sensitivity analysis and the influence of within-cell scale on the between-cell scale on the transmission dynamics) was presented in section 4. The last section contained discussion and conclusion of the study.

2 Formulation of Mathematical Model

We have presented the two submodels which describe the transmission of Hepatitis B virus (HBV) at two different scales (within-cell scale and between-cell scale). The integration of the two scales at the cell-level of biological organisation forms the focus of our model and analysis in this study. We develop :

(a) The within-cell scale submodel dynamics: The study formulated the dynamics of the within-cell scale model, assuming the following five populations to interact : core particle in cytoplasm (h_r), cccDNA inside the nucleus (h_t), complete virions (h_c), incomplete particles (h_i), and within-cell viral load (V_s). While [26] describes a more complex within-cell scale model, this work presents a simplified version that makes a distinction between complete virions and incomplete particles. It employed the law of mass action to describe the movement from one state to another using ordinary differential equations. The following assumptions were made for the within-cell processes:
(i) there is no superinfection in the cell,
(ii) that only the capsids containing mature rcDNA either secreted from the cell or recycle the nucleus to replenish the cccDNA pool,
(iii) the intracellular replication dynamics of the core particle is only captured through the reverse transcription of the initial value in the cytoplasm, $h_c = h_c(0)$.
(iv) the influence of within-cell viral load on assembly and export individual cell infectiousness is proxied by $V_s = V_s(s)$,
(v) the within-cell scale processes occur at fast time scale (s), so that $h_r = h_r(s), h_t = h_t(s), h_c =$

$h_c(s), h_i = h_i(s)$ and $V_s = V_s(s)$. Then, this was derived:

$$
\begin{aligned}
\frac{dh_r(s)}{ds} &= \Lambda_r - \eta_r h_r(s) V_s(s) - \delta_r h_r(s), \\
\frac{dh_t(s)}{ds} &= \eta_r h_r(s) V_s(s) - (\alpha_t + \mu_t + \delta_t) h_t(s), \\
\frac{dh_c(s)}{ds} &= \alpha_t h_t(s) - (\alpha_c + \rho_c) h_c(s), \\
\frac{dh_i(s)}{ds} &= \mu_t h_t(s) - (\alpha_i + \delta_i) h_i(s), \\
\frac{dV_s(s)}{ds} &= N_c \alpha_c h_c(s) + N_i \alpha_i h_i(s) - (r_c + r_i) V_s(s).
\end{aligned}
\tag{2.1}
$$

In the model system (2.1), the dynamics of the core particle internalisation into the nucleus and DNA repair (i.e., the change from rcDNA to cccDNA) are described by the model system's first equation. (Λ_r) represents the source of the mature rcDNA, the second term represents the reaction rate of DNA repair in the nucleus at rate (η_r) and the third term is the degradation rate of core particle in the cytoplasm (δ_r). The second equation in model (2.1) describes the dynamics of transcription from the cccDNA. Following the nuclear import of rcDNA, it undergoes conversion into cccDNA, which serves as a template for the transcription of pgRNA, precore mRNAs, and other subgenomic mRNAs, as noted in [27]. The first term of second equation is the rate of proportion of the cccDNA replenishment through intracellular replication while the second term represents the transcription rate of DNA to RNA code, the third term is transcription rate of mRNAs and the last term is the degradation rate of cccDNA.

In the model system (2.1), the third equation describes the dynamics of the translation of pgRNA that leads to the formation of complete virion. The first term of the equation α_t represents the template from the cccDNA, the second term of the equation is association rate of pregenome-polymerase complex (RNP) and core protein, the third term is the translation rate of pgRNA to reverse trancription and the last term is recycling rate of mature rcDNA that leads to the amplification of cccDNA pool in the nucleus. The fourth equation of the system (2.1) describes the translation of subgenomic RNA (mRNA) that leads to the formation of incomplete particles [that is the RNA containing particles, empty virions and subviral particles (SVPs)]. The first term represents the transcription rate of mRNAs, the second term is translation rate of mRNAs and the last term is the degradation rate of mRNAs.

The last equation of the model system (2.1) describes the dynamics of the viral load (particles and proteins within the cytoplasm). The envelopment and release of both complete virions and incomplete particles, such as mature core particles or nucleocapsids, can occur through two pathways. These particles have two possible fates: they can either be recycled back to the nucleus or get enveloped by going through the pre-Golgi compartment and post-endoplasmic reticulum and released as virions into the circulation as described in [27]. The first term represents the association rate of core particle and surface protein that is the source of infectious and non-infectious molecules inside the cytoplasm. The second and third term represent release rate of progeny virions into the extracellular space and the release rate of incomplete particles into the extra cellular space. The figure below shows the parameters of the model and their description.

(b) The between-cell scale submodel dynamics: In this section, we developed a mathematical model for describing Hepatitis B transmission dynamics at the macroscale (between-cell scale) and is described by an SI model. It consists of the population of susceptible (S_C) and infected cells (I_C) so that the total cell population is given $N_C = S_C + I_C$. The following assumptions were made for the between-cell model :

(i) The infected cell does not become immune to the infection.

(ii) The number of infected cells determines the transmission parameter β_C, so that $\beta_C = \beta_C(I_C)$.

(iii) The transmission dynamics of both cells are assumed to occur at a slow time scale so that $S_C = S_C(t)$, $I_C = I_C(t)$ and $V_C = V_C(t)$.

$$
\begin{aligned}
\frac{dS_C(t)}{dt} &= \Lambda_C - \beta_C(I_C)S_C(t) - \mu_C S_C(t) \\
\frac{dI_C(t)}{dt} &= \beta_C(I_C)S_C(t) - (\mu_C + d_C)I_C(t)
\end{aligned}
\tag{2.2}
$$

(c) The multiscale model dynamics: The two submodels which describe the transmission of HBV at both scales that is within - cell scale (a) and between - cell scale (b) were integrated. In this section, the mathematical model and analysis centre on the integration of the two scales at the cell level of biological organisation. Nested multiscale model for Hepatitis B viral infections that consider the intracellular and extracellular dynamics at the cell level was developed based on the mathematical framework presented in [25]. The transmission parameter in the between-cell scale presented in (b) is now a function of both the infected cell population and the within-cell virus variable. Thus $\bar{\beta}(I_C) = \bar{\beta}[V_s(s)I_C(t)]$, which represents a function of the product of within-cell scale viral load and the population of the infected cells. This can be denoted as $V_C(t)$ which is the total infectiousness of the multiscale model as known as "Community Viral Load" that is $V_C(t) = V_s(s)I_C(t)$.

Therefore $\bar{\beta}_C = \bar{\beta}_C(V_C(t))$. Holling type II functional form is applied in order to make the force of infection associated with the infectivity to the cells at this scale, $\lambda_C(t)$, become:

$$
\lambda_C(t) = \bar{\beta}_C(V_C(t)) = \frac{\beta_C V_C(t)}{V_0 + V_C(t)}
$$

At any time t, a total of $I_C(t)$ infected cells, each with an average of $V_s(s)$ virions, was arrived at. Therefore, the rate of change of $V_C(t)$ in the entire hepatocyte, composed of $I_C(t)$ cells, which are homogeneous and unevenly distributed within the hepatocytes, can be expressed as:

$$
\frac{dV_C(t)}{dt} = V_s(s)r_c I_C(t) - \sigma(V_s, h_r)V_C(t)
\tag{2.3}
$$

The derivations and assumptions from the within - cell model (2.1), the between - cell model (2.2)

and (2.3) made up of the multiscale model for HBV cell to cell and is given as :

$$
\begin{aligned}
\frac{dh_r(s)}{ds} &= \Lambda_r - \eta_r h_r(s) V_s(s) - \delta_r h_r(s), \\
\frac{dh_t(s)}{ds} &= \eta_r h_r(s) V_s(s) - (\alpha_t + \mu_t + \delta_t) h_t(s), \\
\frac{dh_c(s)}{ds} &= \alpha_t h_t(s) - (\alpha_c + \rho_c) h_c(s), \\
\frac{dh_i(s)}{ds} &= \mu_t h_t(s) - (\alpha_i + \delta_i) h_i(s), \\
\frac{dV_s(s)}{ds} &= N_c \alpha_c h_c(s) + N_i \alpha_i h_i(s) - (r_c + r_i) V_s(s), \\
\frac{dS_C(t)}{dt} &= \Lambda_C - \frac{\beta_C V_C(t) S_C(t)}{V_0 + V_C(t)} - \mu_C S_C(t), \\
\frac{dI_C(t)}{dt} &= \frac{\beta_C V_C(t) S_C(t)}{V_0 + V_C(t)} - (\mu_C + d_C) I_C(t), \\
\frac{dV_C(t)}{dt} &= V_s(s) r_c I_C(t) - \sigma_C V_C(t).
\end{aligned}
\tag{2.4}
$$

The within-cell scale influences the between-cell scale by shedding / excretion of the pathogen (virus) and the between-cell scale influences the within-cell scale by initial infection of the pathogen (virus). It should be mentioned that the within-cell scale submodel timeframe and the between-cell scale submodel timescale have different time scales. The time scale in the within-cell submodel is (s) is faster than the between-cell submodel (t). In order to analyse the model system (2.4), we apply a singular perturbation (slow and fast time scale analysis) to model system (2.4). Rewriting the submodel system by relation $t = \epsilon s$, where $0 < \epsilon \ll 1$, allows the consideration of the within-cell submodel, which is the replication dynamics submodel. As a result, the within-cell scale submodel becomes:

$$
\begin{aligned}
\epsilon \frac{dh_r(t)}{dt} &= \Lambda_r - \eta_r h_r(t) V_s(t) - \delta_r h_r(t), \\
\epsilon \frac{dh_t(t)}{dt} &= \eta_r h_r(t) V_s(t) - (\alpha_t + \mu_t + \delta_t) h_t(t), \\
\epsilon \frac{dh_c(t)}{dt} &= \alpha_t h_t(t) - (\alpha_c + \rho_c) h_c(t), \\
\epsilon \frac{dh_i(t)}{dt} &= \mu_t h_t(t) - (\alpha_i + \delta_i) h_i(t), \\
\epsilon \frac{dV_s(t)}{dt} &= N_c \alpha_c h_c(t) + N_i \alpha_i h_i(t) - (r_c + r_i) V_s(t).
\end{aligned}
\tag{2.5}
$$

The within-cell scale submodel's fast time scale contrasts with the between-scale transmission dynamics submodel's slow time scale in the within-cell scale model system (2.4), where ϵ is a constant. Given that $0 < \epsilon \ll 1$, we set $\epsilon = 0$ to make the within-cell scale of HBV replication dynamics

independent of time, which is simplified to algebraic equations in (2.5).

$$
\begin{aligned}
\Lambda_r - \eta_r \tilde{h}_r \tilde{V}_s - \delta_r \tilde{h}_r &= 0, \\
\eta_r \tilde{h}_r \tilde{V}_s - (\alpha_t + \mu_t + \delta_t)\tilde{h}_t &= 0, \\
\alpha_t \tilde{h}_t - (\alpha_c + \rho_c)\tilde{h}_c &= 0, \\
\mu_t \tilde{h}_t - (\alpha_i + \delta_i)\tilde{h}_i &= 0, \\
N_c \alpha_c \tilde{h}_c + N_i \alpha_i \tilde{h}_i - (r_c + r_i)\tilde{V}_s &= 0.
\end{aligned}
\tag{2.6}
$$

Solving (2.6), it is derived that:

$$
\tilde{h}_r = \frac{\Lambda_r}{\delta_r \Re_0},
$$

$$
\tilde{h}_t = \frac{\delta_r(\alpha_c + \rho_c)(\alpha_i + \delta_i)(r_c + r_i)}{\eta_r[N_c \alpha_c \alpha_t(\alpha_i + \delta_i) + N_i \alpha_i \mu_t(\alpha_c + \rho_c)]}[\Re_0 - 1],
$$

$$
\tilde{h}_c = \frac{\delta_r \alpha_t(\alpha_i + \delta_i)(r_c + r_i)}{\eta_r[N_c \alpha_c \alpha_t(\alpha_i + \delta_i) + N_i \alpha_i \mu_t(\alpha_c + \rho_c)]}[\Re_0 - 1],
$$

$$
\tilde{h}_i = \frac{\delta_r \mu_t(\alpha_c + \rho_c)(r_c + r_i)}{\eta_r[N_c \alpha_c \alpha_t(\alpha_i + \delta_i) + N_i \alpha_i \mu_t(\alpha_c + \rho_c)]}[\Re_0 - 1],
$$

$$
\tilde{V}_s = \frac{\delta_r}{\eta_r}[\Re_0 - 1]
$$

$\tilde{V}_s$ is the viral load of the within-cell submodel.
where:

$$
\Re_0 = \frac{\Lambda_r \eta_r[N_c \alpha_c \alpha_t(\alpha_i + \delta_i) + N_i \alpha_i \mu_t(\alpha_c + \rho_c)]}{\delta_r(\alpha_t + \mu_t + \delta_t)(\alpha_c + \rho_c)(\alpha_i + \delta_i)(r_c + r_i)}
$$

$\Re_0$ is the basic reproduction number of the within-cell scale. The simplified nested multiscale model is obtained by upscaling the within-cell viral load into the community viral load of the between-cell submodel and is given as:

$$
\begin{aligned}
\frac{dS_C(t)}{dt} &= \Lambda_C - \frac{\beta_C V_C(t)S_C(t)}{V_0 + V_C(t)} - \mu_C S_C(t), \\
\frac{dI_C(t)}{dt} &= \frac{\beta_C V_C(t)S_C(t)}{V_0 + V_C(t)} - (\mu_C + d_C(\tilde{V}_s, \tilde{h}_r))I_C(t), \\
\frac{dV_C(t)}{dt} &= \tilde{V}_s r_c I_C(t) - \sigma_C(\tilde{V}_s, \tilde{h}_r)V_C(t).
\end{aligned}
\tag{2.7}
$$

From the multiscale model system (2.7), it was seen that the total infectious reservoirs of cells (CVL) $V_s(s)I_C(t)$ is now approximated $\tilde{V}_s I_C(t)$ (that is the within-cell viral load is now time independent). This can be rewritten in the simplified nested multiscale model as:

$$
\begin{aligned}
\frac{dS_C(t)}{dt} &= \Lambda_C - \frac{\beta_C V_C(t)S_C(t)}{V_0 + V_C(t)} - \mu_C S_C(t), \\
\frac{dI_C(t)}{dt} &= \frac{\beta_C V_C(t)S_C(t)}{V_0 + V_C(t)} - (\mu_C + d_C)I_C(t), \\
\frac{dV_C(t)}{dt} &= N_s r_c I_C(t) - \sigma_C V_C(t).
\end{aligned}
\tag{2.8}
$$

Where the viral clearance rate $\sigma_C = \sigma_C(\tilde{V}_s, \tilde{h}_r)$, a constant parameter; the virus induced death rate $d_C = d_C(\tilde{V}_s, \tilde{h}_r)$, a constant parameter and the within-cell viral load $N_s = \tilde{V}_s$, a composite parameter (that is a parameter that consists of various number of parameters).
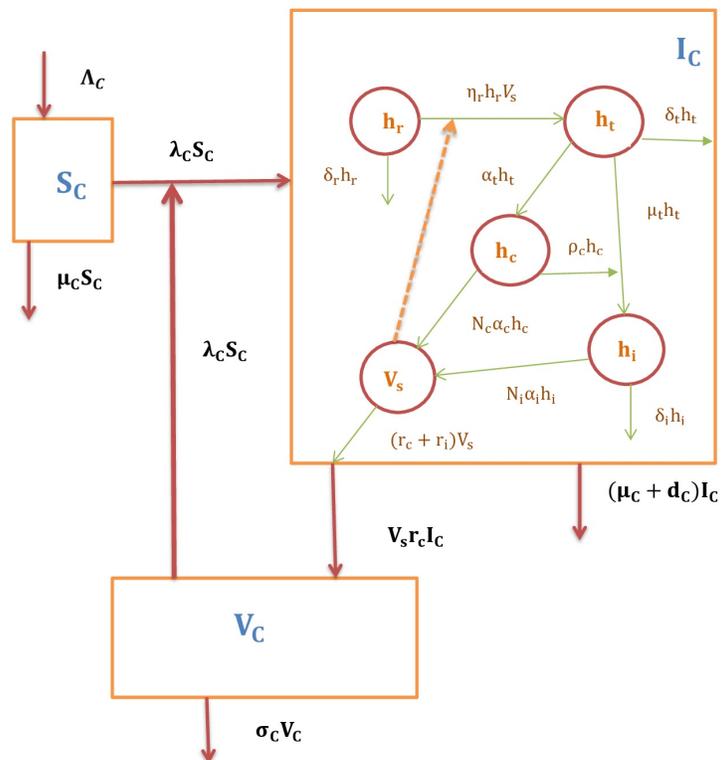

Figure 1: A conceptual diagram of the multiscale model of HBV transmission dynamics

3 Mathematical and Numerical Analysis of the Multiscale Model

The Simplified Nested Multiscale Model (SNMSM) derived in (2.8) will be analysed mathematically and numerically as discussed below.

3.1 Positivity of the solutions of the SNMSM

In order for the model system (2.8) to be realistic, solutions will have to be nonnegative at all times for all $t > 0$. We show that every state variable in the system will remain nonnegative.
Theorem 3.1 : Given that the initial conditions of the model (2.8) remain nonnegative i.e $(S_C(0) \geq 0, I_C(0) \geq 0, V_C(0) \geq 0)$, then the solution set is $(S_C(t), I_C(t), V_C(t))$ is nonnegative for all $t \geq 0$.

Proof : Let $t^* = \sup\{S_C(0) > 0, I_C(0) > 0, V_C(0) > 0\}$

Since $S_C(t), I_C(t)$ and $V_C(t)$ are continuous , we deduce that $t^* > 0$. If $t^* = +\infty$, then positivity holds but if $0 < t^* < +\infty$, $S_C(t) = 0$ or $I_C(t) = 0$ or $V_C(t) = 0$. Now, consider the first equation of the system (2.8),

$$\frac{dS_C(t)}{dt} = \Lambda_C - \frac{\beta_C V_C(t) S_C(t)}{V_0 + V_C(t)} - \mu_C S_C(t)$$

$$\frac{dS_C(t)}{dt} = \Lambda_C - (\lambda_C(t) + \mu_C) S_C(t)$$

$$\frac{dS_C(t)}{dt} + (\lambda_C(t) + \mu_C) S_C(t) = \Lambda_C \qquad (3.1)$$

where $\lambda_C(t) = \frac{\beta_C V_C(t) S_C(t)}{V_0 + V_C(t)}$

Integrating the equation (3.1), thus:

$$\frac{d}{dt}\left\{S_C(t) e^{(\mu_C t + \int \lambda_C(\tau) d\tau)}\right\} = \Lambda_C e^{(\mu_C t + \int \lambda_C(\tau) d\tau)}$$

And:

$$S_C(t^*) e^{(\mu_C t^* + \int_0^{t^*} \lambda_C(\tau) d\tau)} - S_C(0) = \int_0^{t^*} e^{(\mu_C + \lambda_C(t)) dt} \Lambda_C dt$$

which implies that:

$$S_C(t^*) = S_C(0) e^{-(\mu_C t^* + \int_0^{t^*} \lambda_C(\tau) d\tau)} + e^{-(\mu_C t^* + \int_0^{t^*} \lambda_C(\tau) d\tau)} \int_0^{t^*} e^{(\mu_C + \lambda_C(t)) dt} \Lambda_C dt$$

$$S_C(t^*) = k_1 S_C(0) + k_1 \int_0^{t^*} e^{(\mu_C + \lambda_C(t)) dt} \Lambda_C dt > 0$$

where $e^{-(\mu_C t^* + \int_0^{t^*} \lambda_C(\tau) d\tau)} > 0$, $S_C(0) > 0$ and from t^* above, it is arrived at that $V_C(t) > 0$. Therefore the solution $S_C(t^*) > 0$ and hence, $S_C(t^*) \neq 0$.

Considering the second equation to model (2.8):

$$\frac{dI_C(t)}{dt} = \frac{\beta_C V_C(t) S_C(t)}{V_0 + V_C(t)} - (\mu_C + d_C) I_C(t)$$

$$\frac{dI_C(t)}{dt} + (\mu_C + d_C) I_C(t) = \lambda_C(t) S_C(t) \qquad (3.2)$$

Integrating equation (3.2), it is got that:

$$\frac{d}{dt}\left\{I_C(t) e^{\int (\mu_C + d_C) dt}\right\} = \lambda_C(t) S_C(t) e^{\int (\lambda_C + d_C) dt}$$

$$I_C(t^*) e^{(\mu_C + d_C) t^*} - I_C(0) = \int_0^{t^*} e^{\int (\lambda_C + d_C) dt} \lambda_C(t) S_C(t) dt$$

This implies that:

$$I_C(t^*) = I_C(0)e^{-(\mu_C+d_C)t^*} + e^{-(\mu_C+d_C)t^*} \int_0^{t^*} e^{\int(\lambda_C+d_C)dt}\lambda_C(t)S_C(t)dt,$$

$$I_C(t^*) = k_2 I_C(0) + k_2 \int_0^{t^*} e^{\int(\lambda_C+d_C)dt}\lambda_C(t)S_C(t)dt,$$

where $k_2 = e^{-(\mu_C+d_C)t^*} > 0, I_C(0) > 0$ and from above, $S_C(t) > 0$, then the soution $I_C(t^*) > 0$ and hence, $I_C(t^*) \neq 0$. Lastly, the third equation of model (2.8) is :

$$\frac{dV_C(t)}{dt} = N_s r_c I_C(t) - \sigma_C V_C(t)$$

$$\frac{dV_C(t)}{dt} + \sigma_C V_C(t) = N_s r_c I_C(t) \tag{3.3}$$

Integrating equation (3.3), it becomes:

$$\frac{d}{dt}\left\{V_C(t)e^{\int \sigma_C dt}\right\} = N_s r_c I_C(t)e^{\int \sigma_C dt}$$

$$V_C(t^*)e^{\sigma_C t^*} - V_C(0) = \int_0^{t^*} e^{\int \sigma_C dt} N_s r_c I_C(t)dt,$$

This implies that:

$$V_C(t^*) = V_C(0)e^{-\sigma_C t^*} + e^{-\sigma_C t^*}\int_0^{t^*} e^{\int \sigma_C dt} N_s r_c I_C(t)dt,$$

$$V_C(t^*) = k_2 V_C(0) + k_2 \int_0^{t^*} e^{\int \sigma_C dt} N_s r_c I_C(t)dt,$$

where $k_2 = e^{-\sigma_C t^*} > 0, V_C(0) > 0$ and from above, $I_C(t) > 0$. So the solution $V_C(t^*) > 0$ and $V_C(t^*) \neq 0$.
Thus, when starting with nonnegative initial value conditions in the model system (2.8), the solutions of the model will remain nonnegative for all $t \geq 0$, and this complete the proof.

3.2 Invariant Region of the Equilibrium of the SNMSM

It is assumed that the parameters of the multiscale model system (2.8) are non negative.

$$\frac{d(S_C(t) + I_C(t))}{dt} = \Lambda_C - \mu_C S_C(t) - (\mu_C + d_C)I_C(t),$$

$$\frac{dN_C(t)}{dt} = \Lambda_C - \mu_C N_C(t) - d_C I_C(t),$$

$$\leq \Lambda_C - \mu_C N_C(t)$$

This implies that:

$$\lim_{t\to\infty} \sup(N_C(t)) = \frac{\Lambda_C}{\mu_C} \tag{3.4}$$

Since $S_C(t)$ and $I_C(t)$ are subsets of $N_C(t)$ and $N_C(t)$ is also bounded above following the result obtained in (3.4), it can concluded using the Bolzano Weierstrass Theorem that $S_C(t)$ and $I_C(t)$ are bounded above. That is, $\lim_{t\to\infty} \sup(S_C(t)) = \frac{\Lambda_C}{\mu_C}$ and $\lim_{t\to\infty} \sup(I_C(t)) = \frac{\Lambda_C}{\mu_C}$. Also,

$$\frac{dV_C(t)}{dt} = N_s r_c I_C(t) - \sigma_C V_C(t),$$

$$\frac{dV_C(t)}{dt} \leq N_s r_c \frac{\Lambda_C}{\mu_C} - \sigma_C V_C(t),$$

$$\lim_{t\to\infty} \sup(V_C(t)) = \frac{N_s r_c \Lambda_C}{\sigma_C \mu_C}.$$

The invariant region is:

$$\Omega = \{S_C(t), I_C(t), V_C(t) \in \mathbb{R}_+^3; N_C(t) \leq \frac{\Lambda_C}{\mu_C}, V_C(t) \leq \frac{N_s r_c \Lambda_C}{\sigma_C \mu_C}\}$$

Since every trajectory that begins in Ω will stay in Ω for all $t \geq 0$, Ω is a positively invariant and attractive region. From a mathematical and epidemiological perspective, the model (2.8) is well-posed.

3.3 Disease Free Equilibrium and Reproduction Number of SNMSM

The Equilibrium states of the model are obtained by setting the Right Hand Sides (RHS) of the system (2.8) to zeros. Disease Free Equilibrium (DFE) and Endemic Equilibrium (EE) are the two equilibria states that the system accepts. $E^0 = (\frac{\Lambda_C}{\mu_C}, 0, 0)$ represents the DFE state, which occurs when there is no infection in the cell. The endemic equilibrium is represented by $E^* = (S_C^*, I_C^*, V_C^*)$. The Reproduction Number which is one of the necessary and important parameter in the analysis of disease outbreak is defined and calculated for the model system (2.8). Within a completely susceptible population, the Reproduction Number ($\mathbb{R}_0$) indicates the anticipated number of secondary cases that an average infected individual will produce during the course of the infection [28]. The next generation approach [29] can be used to determine the Reproduction Number in the following manner:

$$\begin{cases} \frac{dX}{ds} = f(X, Y, Z), \\\\ \frac{dY}{ds} = g(X, Y, Z), \\\\ \frac{dZ}{ds} = h(X, Y, Z) \end{cases}$$

where:

$$\begin{cases} X = (h_r, S_C), \\\\ Y = (h_t, h_c, h_i, I_C), \\\\ X = (V_s, V_C) \end{cases}$$

The number of susceptibles, the number of infected, and the number of cell capable of spreading the virus are represented by the components of X, Y, and Z, respectively. Thus:

$$\tilde{g}_1(X^*, Z) = \frac{\beta_C \Lambda_C Z}{\mu_C(\mu_C + d_C)(V_0 + Z)},$$

Unless otherwise indicated, it is assumed that $\Lambda_C > \mu_C$ in all that follows:

$$h(X^*, \tilde{g}(X^*, Z), Z) = \frac{N_s r_c \beta_C \Lambda_C Z}{\mu_C(\mu_C + d_C)(V_0 + Z)} - \sigma_C Z,$$

Assume that A can also be expressed as $A = M - D$, where $M \geq 0$ and $D > 0$. Let $A = D_Z h(X^*, \tilde{g}(X^*, 0), 0)$.

$$D_z h(h^*, \tilde{g}(X^*, 0), 0) = \frac{N_s r_c \beta_C \Lambda_C}{\mu_C(\mu_C + d_C)V_0} - \sigma_C,$$

$$M = \frac{N_s r_c \beta_C \Lambda_C}{\mu_C(\mu_C + d_C)V_0},$$

$$D = \sigma_C,$$

$$MD^{-1} = \frac{N_s r_c \beta_C \Lambda_C}{\sigma_C \mu_C(\mu_C + d_C)V_0}.$$

The spectral radius, or dominant eigenvalue, of the matrix MD^{-1} is the fundamental reproduction number, that is

$$\mathbb{R}_0 = \rho(MD^{-1})$$

$$\mathbb{R}_0 = \frac{N_s r_c \beta_C \Lambda_C}{\sigma_C \mu_C(\mu_C + d_C)V_0} \tag{3.5}$$

The basic Reproduction Number of the multiscale model (2.8) can expressed as two different components as shown below:

$$\mathbb{R}_0 = \mathbb{R}_{0R}.\mathbb{R}_{0T}$$

$$\mathbb{R}_0 = \frac{N_s r_c}{(\mu_C + d_C)} \times \frac{\beta_C \Lambda_C}{\sigma_C \mu_C V_0}$$

(i) Consider a single newly complete virion entering HBV virus- free community / environment at an equilibrium point. The entire discharged virion is still there and contagious. $\mathbb{R}_{0R}$ is the anticipated amount of infectiousness that was provided during the whole infection time. That is

$$\mathbb{R}_{0R} = \frac{N_s r_c}{(\mu_C + d_C)}$$

This is dependent on the average viral load N_s in the cell, which is expelled or released from the cytoplasm into the cell environment at a rate r_c of an infected cell. During each cell's whole infectiousness period, the virus spreads to other target cells. N_s is a composite quantity that can be expressed as the within-cell scale viral load endemic value.

$$N_s = \frac{\delta_r}{\eta_r}[\Re_0 - 1]$$

where:

$$\Re_0 = \frac{\Lambda_r \eta_r [N_c \alpha_c \alpha_t (\alpha_i + \delta_i) + N_i \alpha_i \mu_t (\alpha_c + \rho_c)]}{\delta_r (\alpha_t + \mu_t + \delta_t)(\alpha_c + \rho_c)(\alpha_i + \delta_i)(r_c + r_i)}$$

The first partial expression for $\mathbb{R}_{0R}$ represents the rate at which an infected cell adds to the Community Viral Load (V_C^*) over the course of its infectiousness, and $\frac{1}{(\mu_C + d_C)}$ represents the infected cell's average life span.

(ii) Comparably, $\mathbb{R}_{0T}$ represents a single newly infectious cell joining an equilibrium community of susceptible cells free of viral burden. That is the approximate number of cells that infectious cells are predicted to infect. Each HBV infection dose is estimated to produce the following number of infected cells :

$$\mathbb{R}_{0T} = \frac{\beta_C \Lambda_C}{\sigma_C \mu_C V_0}$$

The second partial expression for the reproduction number depends on the recruitment rate of susceptible cells Λ_C, the average life span of each susceptible cell $\frac{1}{\mu_C}$, the contact rate of susceptible cells in the infectious environment β_C, the average time taken for the viral clearance in the community / environment $\frac{1}{\sigma_C}$ and the susceptibility coefficient to HBV infection in the cell community $\frac{1}{V_0}$, where V_0 is the Community Viral Load that results in 50% chance of the cell being infected.

The reproduction number ($\mathbb{R}_0$) of the multiscale model system (2.8) is comprised of the within-cell scale parameters and the between-cell scale disease parameters, as expressed in (i) and (ii). According to Theorem 2 of [29], the local stability of the DFE of the multiscale model system (2.8) is assured.

3.4 Global Stability of Disease Free Equilibrium of SNMSM

The next generation operator [30] was applied to ascertained the global stability of DFE of the simplified nested multiscale model system (2.8). The model system can be re-written in the form

$$\begin{cases} \frac{dX}{dt} = F(X, Z), \\ \\ \frac{dZ}{dt} = G(X, Z), G(X, 0) = 0 \end{cases}$$

where $X = (S_C)$; $Z = (I_C, V_C)$ and $(X^*, 0)$ denotes the DFE of the system (2.8). It is assumed that the conditions $(H1)$ and $(H2)$ below are ideal:

(H1): For $\frac{dX}{dt} = F(X, 0), X^*$ is GAS

(H2): $G(X, Z) = AZ - \hat{G}(X, Z), \hat{G}(X, Z) \geq 0, (X, Z) \in \psi$ where $A = D_Z G(X, 0)$ is an M-matrix and ψ is the region where the model makes biological sense. In relation to model (2.8), therefore:

$$F(X, Z) = (\Lambda_C - \frac{\beta_C V_C S_C}{V_0 + V_C} - \mu_C S_C)$$

$$G(X, Z) = \begin{pmatrix} \frac{\beta_C V_C S_C}{V_0 + V_C} - (\mu_C + d_C) I_C \\ \\ N_s r_c I_C - \sigma_C V_C \end{pmatrix}$$

So

$$F(X,0) = (\Lambda_C - \mu_C S_C)$$

and

$$A = \begin{pmatrix} -(\alpha_C + d_C) & \frac{\beta_C \Lambda_C}{\mu_C V_0} \\ N_s r_c & -\alpha_C \end{pmatrix}$$

Using AZ and $G(X,Z)$, it was deduced that:

$$\hat{G}(X,Z) = \begin{pmatrix} (\frac{\Lambda_C}{\mu_C V_0} - \frac{S_C}{V_0 + V_C})\beta_C V_C \\ 0 \end{pmatrix}$$

Since $\frac{\Lambda_C}{\mu_C V_0} \geq \frac{S_C}{V_0 + V_C}$ it is clear that $\hat{G}(X,Z) \geq 0$ for all $(X,Z) \in \mathbb{R}^3_+$. Also, it is noted that A is an M-matrix, as the off-diagonal elements of A A are non-negative. Therefore, the disease-free equilibrium is asymptotically stable globally.

3.5   The Endemic Equilibrium of SNMSM

The Endemic Equilibrium Point of the multiscale model (2.8) denoted as $E^* = (S_C^*, I_C^*, V_C^*)$ and at this point each of the variables are constants and the rate of change of the model variable is zero. The expressions for the endemic equilibrium and their description were derived as follows: From equation (1) of the model system (2.8):

$$S_C^* = \frac{\Lambda_C(V_0 + V_C^*)}{(\beta_C + \mu_C)V_C^* + \mu_C V_0}$$

From equation (2) of the system (2.8) it was derived that:

$$I_C^* = \frac{\beta_C \Lambda_C V_C^*}{(\mu_C + d_C)[(\beta_C + \mu_C)V_C^* + \mu_C V_0]} \tag{3.6}$$

Also, from equation (3) of the model system (2.8), it was got:

$$I_C^* = \frac{\sigma_C V_C^*}{N_s r_c} \tag{3.7}$$

Equating the two expressions (3.6) and (3.7) for I_C^*, it was inferred that the expression for V_C^* was as follows:

$$\frac{\sigma_C V_C^*}{N_s r_c} = \frac{\beta_C \Lambda_C V_C^*}{(\mu_C + d_C)[(\beta_C + \mu_C)V_C^* + \mu_C V_0]} \tag{3.8}$$

Solving equation (3.8), two values for V_C^* were arrived at as follows:

$$\begin{cases} V_C^* = 0, \\ V_C^* = \frac{\mu_C V_0}{\beta_C + \mu_C}[\frac{N_s r_c \beta_C \Lambda_C}{\sigma_C \mu_C (\mu_C + d_C)V_0} - 1]. \end{cases} \tag{3.9}$$

The first solution for V_C^* denoted the value of the Disease Free Equilibrium and the second value is the Endemic value of the system (2.8). Substituting the value of the reproduction number to the

second value of V_C^*, it was derived that the following expressions for the Endemic Equilibrium were as follows:

$$
\begin{aligned}
S_C^* &= \frac{\Lambda_C(\beta_C + \mu_C \mathbb{R}_0)}{\mu_C(\beta_C + \mu_C)\mathbb{R}_0}, \\
I_C^* &= \frac{\Lambda_C \beta_C(\mathbb{R}_0 - 1)}{(\mu_C + d_C)(\beta_C + \mu_C)\mathbb{R}_0},
\end{aligned}
\tag{3.10}
$$

$$
V_C^* = \frac{\mu_C V_0}{(\beta_C + \mu_C)}(\mathbb{R}_0 - 1).
\tag{3.11}
$$

where

$$
\mathbb{R}_0 = \frac{N_s r_c \beta_C \Lambda_C}{\sigma_C \mu_C(\mu_C + d_C)V_0}
\tag{3.12}
$$

It is clear that the expressions of (3.11) and (3.12) that the single positive endemic equilibrium point for the model system (2.8) exist for $\mathbb{R}_0 > 1$ and whenever $\Re_0 > 1$. Accordingly, it was deduced that the model (2.8) has a single distinct endemic equilibrium point. The results obtained above can be summarised by stating the following theorem.

3.6 Local Stability of the Endemic Equilibrium of SNMSM

The following theorem illustrates how we will use the [31] to model (2.8) in order to determine the local stability of the endemic equilibrium.

Theorem (3.6): Consider the following general system of Ordinary Differential Equations with parameter ϕ:

$$
\frac{dx}{dt} f(x, \phi), f : \mathbb{R}^n \longrightarrow \mathbb{R}, f : \mathbb{C}^2(\mathbb{R}^2 \times \mathbb{R})
\tag{3.13}
$$

where 0 is an equilibrium point of the system (2.8), (i.e $f(0, \phi)$), $\forall \phi$, and assume that

(i) $A = D_x f(0, 0) = (\frac{\partial f_i(0,0)}{\partial x_i})$ is a linearization of the system around the equilibrium 0 with ϕ evaluated at 0;

(ii) zero is a simple eigenvalue of A and other eigenvalues of A have negative real part;

(iii) Matrix A has a left eigenvector denoted by v and a right eigenvector denoted by u, corresponding to the zero eigenvalue.

Let f_k be the kth component of f and

$$
\begin{aligned}
a &= \sum_{k,i,j=1}^n u_k v_i v_j \frac{\partial^2 f_k}{\partial x_i \partial x_j}(0, 0), \\
b &= \sum_{k,i=1}^n u_k v_i \frac{\partial^2 f_k}{\partial x_i \partial \phi}(0, 0),
\end{aligned}
\tag{3.14}
$$

The local dynamics of the system around the equilibrium point 0 is totally governed by the signs of a and b.

(i) $a > 0, b > 0$, when $\phi < 0$ with $|\phi| \ll 1$, 0 is LAS, and there exists a positive unstable equilibrium; when $0 < \phi < 1$, 0 is unstable and there exists a negative and locally asymptotically stable equilibrium.

(ii) $a < 0, b < 0$, when $\phi < 0$ with $|\phi| \ll 1$, 0 is unstable ; when $0 < \phi \ll 1$, 0 is LAS, and there exists a positive unstable equilibrium point.

(iii) $a > 0, b < 0$, when $\phi < 0$ with $|\phi| \ll 1$, 0 is unstable and there exists a LAS negative equilibrium; when $|\phi| \ll 1$, 0 is stable and a positive unstable equilibrium appear.

(iv) $a < 0, b > 0$, when ϕ changes from negative to positive, 0 changes its stability from stable to unstable. Correspondingly a negative unstable equilibrium becomes positive and LAS.

In this case, the Center Manifold Theorem as stated above was applied by making the following change of variables $S_C = x_1, I_C = x_2, V_C = x_3$. Further, it is allowed that $\phi = \beta^*$, where β^* is a bifurcation parameter. If $\beta^* = \beta_C$ and $\mathbb{R}_0 = 1$, and solve for β^*,

$$\beta^* = \frac{\sigma_C \mu_C V_0 (\mu_C + d_C)}{N_s r_c \Lambda_C}$$

In addition, the vector notation $x = (x_1, x_2, x_3)^T$ was employed. This allows the expression of the model system (2.8) as $\frac{dx}{dt} = F(x, \beta^*)$, where $F = (f_1, f_2, f_3)$.

$$
\begin{aligned}
\dot{x_1} &= \Lambda_C - \frac{\beta^* x_3 x_1}{V_0 + x_3} - \mu_C x_1, \\
\dot{x_2} &= \frac{\beta^* x_3 x_1}{V_0 + x_3} - (\mu_C + d_C) x_2, \\
\dot{x_3} &= N_s r_c x_2 - \sigma_C x_3.
\end{aligned}
\tag{3.15}
$$

The system of equation (3.15) evaluated at the DFE (E^0) has the following Jacobian matrix:

$$
A = \begin{pmatrix}
-\mu_C & 0 & -\frac{\beta^* \Lambda_C}{\mu_C V_0} \\
0 & -(\mu_C + d_C) & \frac{\beta^* \Lambda_C}{\mu_C V_0} \\
0 & N_s r_c & -\sigma_C
\end{pmatrix}
\tag{3.16}
$$

Solving the eigenvalues for this new Jacobian matrix with β_C replaced by the expression for β^* and solving for the eigenvalues yields the following values of λ:

$$
\begin{cases}
\lambda_1 = 0, \\
\lambda_2 = -\mu_C, \\
\lambda_3 = -(\sigma_C + \mu_C + d_C)
\end{cases}
$$

As can be seen from the preceding result, the linearised system of the transformed equation (3.15) with β^* as the bifurcation point has a simple zero eigenvalue. The dynamics of the system (3.15) at $\beta_C = \beta^*$ can therefore be examined using the center manifold theorem.

The left eigenvector associated with the zero eigenvalue of the model system (3.15) is $u = (u_1, u_2, u_3)^T$, which is the Jacobian matrix value, where:

$$
\begin{cases}
u_1 = -\frac{\beta^* \Lambda_C}{\mu_C^2 V_0}, \\
u_2 = \frac{\sigma_C}{N_s r_c} = \frac{\beta^* \Lambda_C}{\mu_C (\mu_C + d_C) V_0}, \\
u_3 = 1.
\end{cases}
\tag{3.17}
$$

The right eigenvector given by $v = (v_1, v_2, v_3)$, where:

$$\begin{cases} v_1 = 0, \\ v_2 = \frac{N_s r_c}{(\mu_C + d_C)}, \\ v_3 = 1. \end{cases} \tag{3.18}$$

Computation of the bifurcation parameters a and b: To find the sign of a, the non-zero second order derivatives at $(0, 0)$ is evaluated in order to assess the non-zero second order derivative of F with respect to each variable, these were obtained:

$$\begin{cases} \frac{\partial^2 f_1}{\partial x_1 \partial x_3}(0,0) = -\frac{\beta^*}{V_0}, \\ \frac{\partial^2 f_1}{\partial x_3 \partial x_1}(0,0) = -\frac{\beta^*}{V_0}, \\ \frac{\partial^2 f_1}{\partial x_3^2}(0,0) = \frac{2\Lambda_C \beta^*}{\mu_C V_0^2}, \\ \frac{\partial^2 f_1}{\partial x_1 \partial x_3}(0,0) = \frac{\beta^*}{V_0}, \\ \frac{\partial^2 f_1}{\partial x_3 \partial x_1}(0,0) = \frac{\beta^*}{V_0}, \\ \frac{\partial^2 f_1}{\partial x_3^2}(0,0) = -\frac{2\Lambda_C \beta^*}{\mu_C V_0^2} \end{cases} \tag{3.19}$$

The sign of the bifurcation constant a is determined as follows:

$$a = u_1 v_3^2 \frac{\partial^2 f_1}{\partial x_3^2}(0,0) + u_2 v_3^2 \frac{\partial^2 f_2}{\partial x_3^2}(0,0)$$

$$a = -\frac{2\Lambda_C \beta^*}{\mu_C V_0^2}\left(\frac{\beta^* \Lambda_C}{\mu_C^2 V_0} + \frac{\sigma_C}{N_s r_c}\right) < 0$$

To determine the sign of b, the following non-vanishing second order derivatives of the transformed model (3.15) were computed, evaluating the non-zero second order derivatives at $(0, 0)$, thus arriving at :

$$\begin{cases} \frac{\partial^2 f_1}{\partial x_1 \partial \beta^*}(0,0) = 0, \\ \frac{\partial^2 f_1}{\partial x_3 \partial \beta^*}(0,0) = -\frac{\Lambda_C}{\mu_C V_0}, \\ \frac{\partial^2 f_2}{\partial x_1 \partial \beta^*}(0,0) = 0, \\ \frac{\partial^2 f_2}{\partial x_3 \partial \beta^*}(0,0) = \frac{\Lambda_C}{\mu_C V_0} \end{cases} \tag{3.20}$$

The sign of the bifurcation constant b is determined as follows:

$$b = u_1 v_3 \frac{\partial^2 f_1}{\partial x_3 \partial \beta^*}(0,0) + u_2 v_3 \frac{\partial^2 f_2}{\partial x_3 \partial \beta^*}(0,0)$$

$$b = \frac{\Lambda_C^2 \beta^*}{\mu_C^2 V_0^2}\left(\frac{1}{\mu_C} + \frac{1}{\mu_C + d_C}\right) > 0$$

Thus $a < 0$ and $b > 0$. Using the theorem (3.6) item (iv), the following result which holds for $\mathbb{R}_0 > 1$ but close to 1 was established.

3.7 Global Stability of the Endemic Equilibrium of SNMSM

Theorem 3.7 : The endemic equilibrium of the model (2.8) is globally asymptotically stable (GAS) whenever $\mathbb{R}_0 > 1$.

Proof : Given a Volterra-type Lyapunov function

$$L_1 = L(S_C, I_C, V_C)$$

$$L_1 = S_C - S_C^* \ln S_C + I_C - I_C^* \ln I_C + c_1(V_C - V_C^* \ln V_C)$$

It is known that $L_1 = 0$ when $(S_C, I_C, V_C) = (S_C^*, I_C^*, V_C^*)$ and $L > 0$ otherwise : L is also radially unbounded. L_1 was differentiated with respect to t in order to get a negative value of L.

$$\dot{L}_1 = (1 - \frac{S_C^*}{S_C})\frac{dS_C}{dt} + (1 - \frac{I_C^*}{I_C})\frac{dI_C}{dt} + c_1(1 - \frac{V_C^*}{V_C})\frac{dV_C}{dt}$$

$$= (1 - \frac{S_C^*}{S_C})[\Lambda_C - \frac{\beta_C V_C S_C}{V_0 + V_C} - \mu_C S_C] + (1 - \frac{I_C^*}{I_C})[\frac{\beta_C V_C S_C}{V_0 + V_C} - (\mu_C + d_C)I_C] + c_1(1 - \frac{V_C^*}{V_C})[N_s r_c I_C - \sigma_C V_C]$$

this can be transformed to:

$$\dot{L}_1 = \quad (1 - \frac{S_C^*}{S_C})[\frac{\beta_C V_C^* S_C^*}{V_0 + V_C^*} + \mu_C S_C^* - \frac{\beta_C V_C S_C}{V_0 + V_C} - \mu_C S_C] + (1 - \frac{I_C^*}{I_C})$$
$$[\frac{\beta_C V_C S_C}{V_0 + V_C} - \frac{\beta_C V_C^* S_C^* I_C}{(V_0 + V_C^*)I_C^*}] + c_1(1 - \frac{V_C^*}{V_C})[N_s r_c I_C - \frac{N_s r_c I_C^* V_C}{V_C^*}]$$

$$\dot{L}_1 = \quad 2\frac{\beta_C V_C^* S_C^*}{V_0 + V_C^*} + \mu_C S_C^* - \mu_C S_C - \frac{\beta_C V_C^*(S_C^*)^2}{(V_0 + V_C^*)S_C} - \frac{\mu_C (S_C^*)^2}{S_C} + \frac{\beta_C V_C S_C^*}{V_0 + V_C} + \mu_C S_C^*$$
$$- \frac{\beta_C V_C^* S_C^* I_C}{(V_0 + V_C^*)I_C^*} - \frac{\beta_C V_C S_C I_C^*}{(V_0 + V_C)I_C} + c_1 N_s r_c I_C - \frac{c_1 N_s r_c I_C^* V_C}{V_C^*} - \frac{c_1 N_s r_c I_C V_C^*}{V_C} + c_1 N_s r_c I_C^*$$

further simplification yields:

$$= \quad -\frac{\mu_C}{S_C}(S_C - S_C^*)^2 - \frac{\beta_C V_C^*(S_C^*)^2}{(V_0 + V_C^*)S_C} + 2\frac{\beta_C V_C^* S_C^*}{V_0 + V_C^*} + \frac{\beta_C V_C S_C^*}{V_0 + V_C} - \frac{\beta_C V_C S_C I_C^*}{(V_0 + V_C)I_C}$$
$$+ [c_1 N_s r_c - \frac{\beta_C V_C^* S_C^*}{(V_0 + V_C^*)I_C^*}]I_C - \frac{c_1 N_s r_c I_C^* V_C}{V_C^*} - \frac{c_1 N_s r_c I_C V_C^*}{V_C} + c_1 N_s r_c I_C^*$$

c_1 was chosen such that:

$$c_1 N_s r_c - \frac{\beta_C V_C^* S_C^*}{(V_0 + V_C^*)I_C^*} = 0$$

This implies that:

$$c_1 = \frac{\beta_C V_C^* S_C^*}{N_s r_c(V_0 + V_C^*)I_C^*}$$

85

So

$$\dot{L_1} = -\frac{\mu_C}{S_C}(S_C - S_C^*)^2 + 3\frac{\beta_C V_C^* S_C^*}{V_0 + V_C^*} - \frac{\beta_C V_C^*(S_C^*)^2}{(V_0 + V_C^*)S_C} - \frac{\beta_C V_C S_C^*}{V_0 + V_C} - \frac{\beta_C V_C S_C I_C^*}{(V_0 + V_C)I_C}$$
$$- \frac{\beta_C (V_C^*)^2 S_C^* I_C}{(V_0 + V_C^*)V_C I_C^*} + \frac{\beta_C V_C S_C^*}{V_0 + V_C^*}$$

$$= \frac{\beta_C V_C^* S_C^*}{V_0 + V_C^*}[3 - \frac{S_C^*}{S_C} - \frac{V_C}{V_C^*} - \frac{I_C V_C^*}{I_C^* V_C}] + \frac{\beta_C V_C S_C^*}{V_0 + V_C}[1 - \frac{S_C I_C^*}{S_C^* I_C}] - \frac{\mu_C}{S_C}(S_C - S_C^*)^2$$

It is known that $1 - \frac{S_C I_C^*}{S_C^* I_C} \leq 0$ since $\frac{S_C}{S_C^*} \geq 1$ and $\frac{I_C^*}{I_C} \geq 1$. It is found that $\dot{L_1} \leq 0$ by applying the arithmetic - geometric mean inequality, indicating that L_1 is in fact a Lyapunov function. Based on Lasalle's Invariance Principle, It can be inferred that E^* has global asymptotic stability (GAS).

4 Sensitivity Analysis and Numerical Simulation
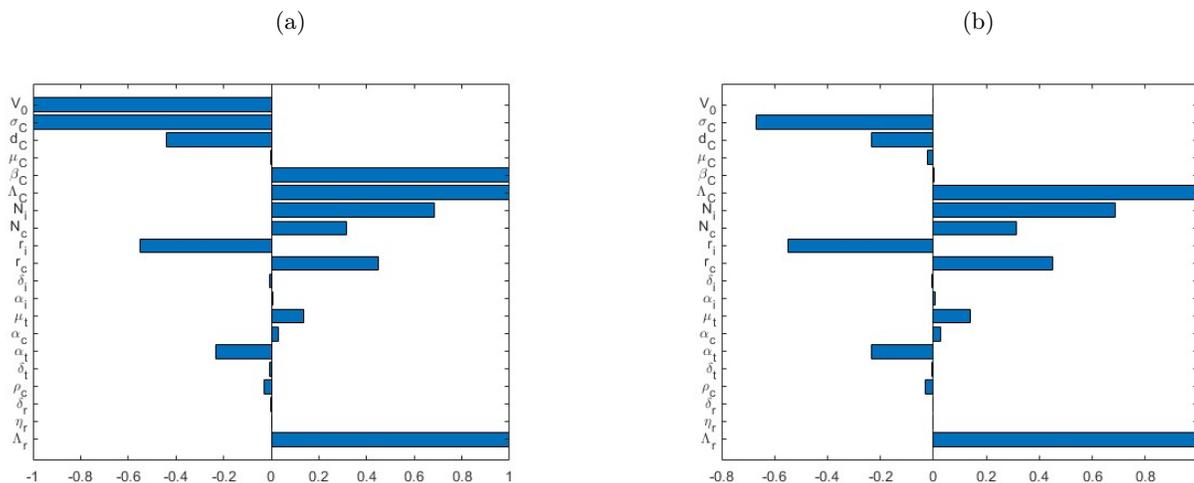
4.1 Sensitivity Analysis

The sensitivity analysis was conducted for the four (4) Hepatitis B transmission metrics (2 at the within-cell scale and the other 2 at the between-cell scale), which will be derived from the multiscale model (2.8). In order to use the multiscale model (2.8) to obtain results that can be used to facilitate the prevention and control of Hepatitis B, Parameters from published literatures were used to parameterise it. At the within-cell scale, the two metrics are: (i) N_s which is the proxy for the individual cell infectiousness and (ii) $\Re_0$ which is the within-cell basic Reproduction Number. The two metrics for the between-cell scales are: (i) V_C^* which is the endemic value of the community viral load and (ii) $\mathbb{R}_0$ is the basic Reproduction Number which is taken as the transmission potential of hepatitis B at the start of the epidemic. The sensitivity analysis of the four metrics $(\Re_0, N_s, \mathbb{R}_0, V_C^*)$ with respect to all the parameters will assist in informing Hepatitis B prevention and treatment policy by using high impact preventions medical interventions since we are at the cell level of organisation. For the 4 Hepatitis B transmission metrics, $(\Re_0, N_s, \mathbb{R}_0, V_C^*)$, the normalised sensitivity index with respect to a parameter P is given by:

$$S_{\Gamma_i}^P = \frac{\partial \Gamma_i}{\partial P} \times \frac{P}{\Gamma_i}, i = \Re_0, N_s, \mathbb{R}_0, V_C^* \tag{4.1}$$

where:

$$\begin{cases} V_C^* = \frac{\mu_C V_0}{(\beta_C + \mu_C)}(\mathbb{R}_0 - 1), \\ \\ \mathbb{R}_0 = \frac{V_s r_c \beta_C \Lambda_C}{\sigma_C \mu_C (\mu_C + d_C) V_0}, \\ \\ N_s = \frac{\delta_r}{\eta_r}(\Re_0 - 1), \\ \\ \Re_0 = \frac{\Lambda_r \eta_r [N_c \alpha_c \alpha_t (\alpha_i + \delta_i) + N_i \alpha_i \mu_t (\alpha_c + \rho_c)]}{\delta r (\alpha_t + \mu_t + \delta_t)(\alpha_c + \rho_c)(\alpha_i + \delta i)(r_c + r_i)}. \end{cases}$$

Figure 2: (a) The normalised sensitivity indices of all the model parameters that influence the HBV transmission metric R_0 in a simplified nested multiscale model.
(b) The normalised sensitivity indices of all the model parameters that influence the HBV transmission metric V_C^* in a simplified nested multiscale model.

The sensitivity analysis results of $\mathbb{R}_0$ and V_C^* to all the baseline model (2.8) parameters in figures 2(a) and 2(b) showed that the majority of the highly sensitive parameters discussed above are the within-cell and between-cell parameters, which justifies the inclusion of within-cell parameters to the overall assessment of the sensitivity of the two transmission metrics from the model (Community Viral Load and Reproduction Number) to the between-cell parameters. This is significant because it helps to identify parameters that are critical for guiding data collection for model parameterisation and to identify parameters that are essential to assessing the efficaciousness of HBV treatment, control, and eliminate. The following results could be deduced:

(i) The parameters with positive will increase the values for both $\mathbb{R}_0$ and V_C^* when they increased, while parameters with negative will decrease the values for both $\mathbb{R}_0$ and V_C^* when they increased. The six parameters $(\beta_C, \Lambda_C, N_i, N_c, r_c, \Lambda_r)$ have a significant impact on the metric $\mathbb{R}_0$. Among the five parameters $(\Lambda_C, N_i, N_c, r_c, \Lambda_r)$, V_C^* has the highest sensitivity; β_C has the lowest sensitivity for V_C^*. Given the significant sensitivity of both $\mathbb{R}_0$ and V_C^* to $(\Lambda_C, N_i, N_c, r_c, \Lambda_r)$, it follows that, in order to improve the validity and reliability of the model system (2.8), care must be taken to ensure that these within-cell and between-cell model parameters are accurate when collecting data.

(ii) The V_C^* is less sensitive to β_C while $\mathbb{R}_0$ is significantly sensitive to β_C, this implies that medical interventions such as Entry Inhibitors, Secretion Inhibitors and direct acting antivirals (DAAs) would have more effect in the control of the transmission of Hepatitis B infection at the cell level at the start of the epidemic than when the virus is already endemic.

4.2 The Infuence of Within-cell Scale on the Between-cell Scale Hepatitis B Transmission Dynamics

To gain a better understanding of the overall behaviour of the pathogens, this section provided numerical simulations of the formulated model using ODE45 solver in Matlab Software Package. The theoretical results derived in section (3.6) were addressed along with the implications of the simulation results, supported by figures. The effect of specific parameters on the between-cell scale variables for the dynamics of Hepatitis B transmission by numerical simulations of the Simplified Nested Multiscale Model system (2.8) were studied. Using analytical techniques, this was demonstrated in subsection (3.6) to show how the within-cell submodel influences the between-cell submodel by demonstrating that the endemic values of the between-cell scale variables are functions of the within-cell scale parameters. The parameter values listed in table 1 are used for the numerical simulations. There are 20 parameters, 14 are within-cell submodel parameters and 6 are between-cell submodel parameters. This section considered the influence of some of the parameters that were relevant in the comparative effectiveness of the treatment and preventive interventions.

Figure 3: (a) Effect of Recruitment rate of rcDNA (Λ_r) on population of susceptible cells for different values of $\Lambda_r : \Lambda_r = 0.00694, \Lambda_r = 0.0694, \Lambda_r = 0.694$ in a SNMSM.
(b) Effect of Recruitment rate of rcDNA (Λ_r) on population of Infected cells for different values of $\Lambda_r : \Lambda_r = 0.00694, \Lambda_r = 0.0694, \Lambda_r = 0.694$ in a SNMSM.
(c) Effect of Recruitment rate of rcDNA (Λ_r) on community viral load for different values of $\Lambda_r : \Lambda_r = 0.00694, \Lambda_r = 0.0694, \Lambda_r = 0.694$ in a SNMSM.

(a)	(b)	(c)
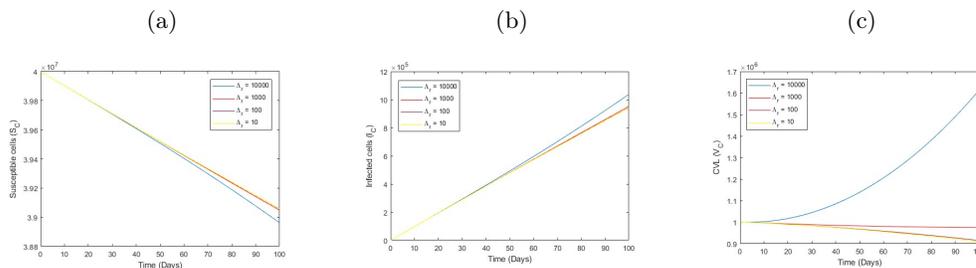
Figures 3(a) to 3(c): show the influence of the variation of the recruitment rate of rcDNA (Λ_r) with $\Lambda_r : \Lambda_r = 0.00694, \Lambda_r = 0.0694, \Lambda_r = 0.694$ on the between-cell scale variable of [population of susceptible cells (S_C), population of infected cells (I_C) and community viral load (V_C)] of model system (2.8). The findings indicated that while there is a little difference in the transmission dynamics of the S_C and I_C, there is an increase in the V_C of the disease on the between-cell scale, as depicted in the above figures, when the recruitment rate of rcDNA (Λ_r) increases. These results predicted that if active control strategies can be put in place at the very first stage of the life cycle of the pathogen at the within-cell scale, the viral load at the within-cell scale and the CVL at the between-cell scale will reduce drastically.

Figure 4: (a) Effect of viral burst size of incomplete particles (N_i) on population of susceptible cells for different values of $N_i : N_i = 0.00139, N_i = 0.0139, N_i = 0.139$ in a SNMSM.
(b) Effect of viral burst size of incomplete particles (N_i) on Prevalence (I_C) for different values of $N_i : N_i = 0.00139, N_i = 0.0139, N_i = 0.139$ in a SNMSM .
(c) Effect of viral burst size of incomplete particles (N_i) on community viral load (V_C), for different values of $N_i : N_i = 0.00139, N_i = 0.0139, N_i = 0.139$ in a SNMSM.
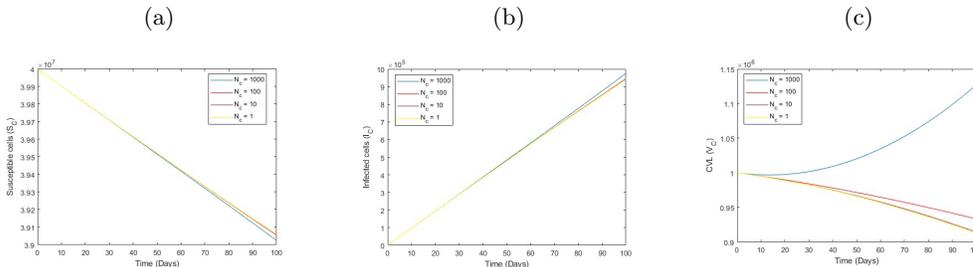
(a) (b) (c)
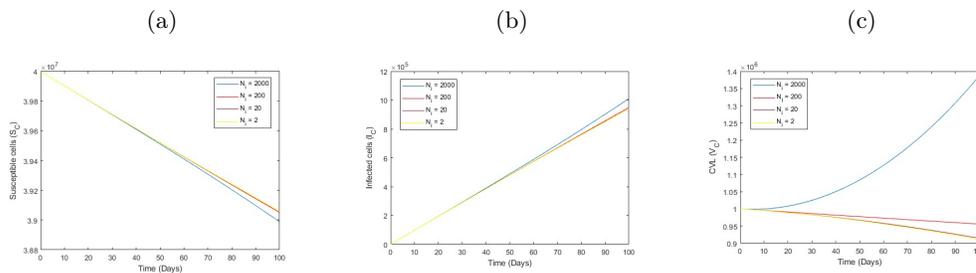
Figures 4(a) to 4(c): show the influence of the variation of the viral burst size of incomplete particles (N_i) with $N_i : N_i = 0.00139, N_i = 0.0139, N_i = 0.139$ on the between-cell scale variable of [population of susceptible cells (S_C), population of infected cells (I_C) and community viral load (V_C)] of model system (2.8). The findings indicated that while there is a modest difference in the susceptible and infected cells, there is an increase in the disease's transmission dynamics in the community viral load with an increase in the viral burst size of incomplete particles (N_i). These findings suggested that control strategies that target replication at the life cycle of the pathogen must be introduced in order to reduce secretion of incomplete particles to the viral load at the within-cell scale and the (community viral load) CVL at the between-cell scale.

Figure 5: (a) Effect of reaction rate of DNA repair (η_r) on population of susceptible cells (S_C) for different values of $\eta_r : \eta_r = 0.00000694, \eta_r = 0.0000694, \eta_r = 0.000694$ in a SNMSM.
(b) Effect of reaction rate of DNA repair (η_r) on population of Infected cells (I_C) for different values of $\eta_r : \eta_r = 0.00000694, \eta_r = 0.0000694, \eta_r = 0.000694$ in a SNMSM.
(c) Effect of reaction rate of DNA repair (η_r) on community viral load (V_C) for different values of $\eta_r : \eta_r = 0.00000694, \eta_r = 0.0000694, \eta_r = 0.000694$ in a SNMSM.

(a)   (b)   (c)
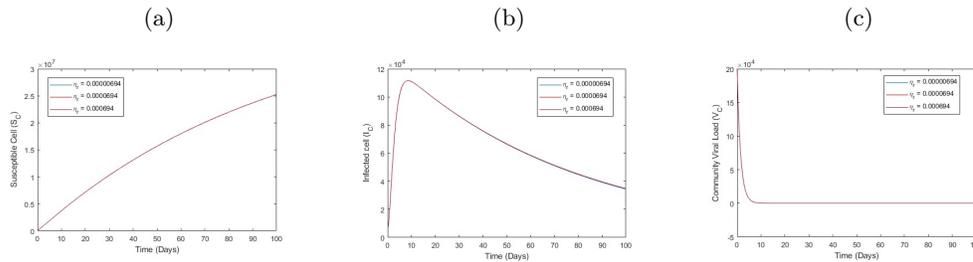
Figures 5(a) to 5(b): show the influence of the variation of the reaction rate of DNA repair (η_r) with $(\eta_r) : (\eta_r) = 0.00000694, (\eta_r) = 0.0000694, (\eta_r) = 0.000694$ on the between-cell scale variable of [population of susceptible cells (S_C), population of infected cells (I_C) and community viral load (V_C)] of model system (2.8). The result shows that an increase in the reaction rate of DNA repair (η_r) makes no difference in the transmission dynamics of the disease in the between-cell scale as its remain constant.

Figure 6: (a) Effect of viral burst size of complete virions (N_c) on population of susceptible cells (S_C) for different values of $N_c : N_c = 0.000694, N_c = 0.00694, N_c = 0.0694$ in a SNMSM.
(b) Effect of reaction rate of DNA repair (N_c) on population of Infected cells (I_C) for different values of $N_c : N_c = 0.000694, N_c = 0.00694, N_c = 0.0694$ in a SNMSM.
(c) Effect of reaction rate of DNA repair (N_c) on community viral load (V_C) for different values of $N_c : N_c = 0.000694, N_c = 0.00694, N_c = 0.0694$ in a SNMSM.

(a)   (b)   (c)

Figures 6(a) to 6(c): show the influence of the variation of the viral burst size of complete virions (N_c) with $N_c : N_c = 0.000694, N_c = 0.00694, N_c = 0.0694$ on the between-cell scale variable

of [population of susceptible cells (S_C), population of infected cells (I_C) and community viral load (V_C)] of model system (2.8). The findings indicated that while there is a modest difference in the transmission dynamics of S_C and I_C, there is an increase in the V_C of the between-cell scale when the viral burst size of incomplete particles (N_c) increases. These results suggested that control strategies that target replication at the life cycle of the pathogen must be introduced in order to reduce excretion of complete virions to the viral load at the within-cell scale and the CVL at the between-cell scale.

5   Discussion and Conclusion

The main contribution of this study to scientific knowledge is the development of Simplified Nested Multiscale Model that: (i) distinguishes between the release of complete virions and incomplete particles from the cytoplasm into the extracellular space at the within-cell submodel. (ii) The study contributes immensely to the development of medical interventions Direct Acting Antivirals (DAAs) toward the improvement of sustained virological response rate of the infected host in the control and the eradication of hepatits B which is one of the leading cause of mortality in the world, especially in the sub-saharan Africa. Another reason for the assumption was the inability most mathematical models of Hepatitis B to give satisfactory response to the eradication of emergence resistance during treatment with DAAs and to treat all genotypes. (iii) we derive advance alternative mathematical modeling for studying hepatic viral infections. In the Simplified Nested Multiscale Model it is only the within-cell parameters that are significant at the endemic state of the disease which explains the unidirectionality of the Simplified Nested Multiscale Model. We were also able to identify through the sensitivity analysis (basic reproductive number and the community viral load) and the numerical simulations of the multiscale models, the main parameters for the eradication of Hepatitis B. However, in the simplified nested multiscale model, the within-cell parameters were upscaled by a composite parameter to the between-cell model. A numerical demonstration of the effects of certain within-cell scales on the between-cell scale was presented, and the benefits of the multiscale model over the single scale model were explored. This study serves as an eye opener to mathematical modelers to be able to integrate different scales at any level of biological organisation as expected. In order to obtain primary data for accurate and clear numerical modeling, we shall make every effort to work in conjunction with scientists in the biological sciences. This study focused on the development and mathematical analysis of the nested multiscale model but in our subsequent publications we will consider the medical interventions that will incorporate the treatments and preventive interventions.

Table 1: Parameters values of model and their description

Parameter	Description	Value/unit	Reference
Λ_r	Recruitment rate of rcDNA	$100\ \text{min}^{-1}$	Assumed
η_r	Reaction rate of DNA repair	0.1min^{-1}	[26]
δ_r	Degradation rate of rcDNA	0.001min^{-1}	[26]
δ_t	Degradation rate of cccDNA	0.001min^{-1}	[26]
ρ_c	Recycling rate of rcDNA	0.01min^{-1}	[26]
α_t	Transcription rate of DNA to RNA code	$0.1\text{molecule}^{-1}\text{min}^{-1}$	[26]
μ_t	Transcription rate of mRNA	$0.1\text{molecule}^{-1}\text{min}^{-1}$	[26]
α_c	Association rate of RNP and core protein	$0.1\text{molecule}^{-1}\text{min}^{-1}$	[26]
α_i	Translation rate of mRNAs	0.1min^{-1}	[26]
δ_i	Degradation rate of mRNAs	0.001min^{-1}	[26]
r_c	Shedding rate of complete virions	0.1min^{-1}	[26]
r_i	Shedding rate incomplete particles	0.1min^{-1}	[26]
N_c	Viral burst size of complete virions	$10\ \text{mins}^{-1}$	Assumed
N_i	Viral burst size of incomplete particles	$20\ \text{mins}^{-1}$	Assumed
Λ_C	Recruitment rate of cell	$4 \times 10^5\ \text{per ml}$	[32]
β_C	Transmission rate	$0.70\ day^{-1}$	Assumed
μ_C	Natural death rate	$0.01\ day^{-1}$	[33]
d_C	Virus induced death rate	$0.003\ day^{-1}$	[33]
V_0	Half saturation constant	$10^6\ \text{virus}\ day^{-1}$	Assumed
σ_C	Natural viral clearance rate	$0.67\ day^{-1}$	[34]

References

[1] P. Van den Driessche. Reproduction numbers of infectious disease models. *Infectious Disease Modelling*, 2(3):288–303, 2017.

[2] X. Wang and J. Wang. Disease dynamics in a coupled cholera model linking within-host and between-host interactions. *Journal of Biological Dynamics*, 11(sup1):238–262, 2017.

[3] L. L. Boeijen, R. C. Hoogeveen, A. Boonstra, and G. M. Lauer. Hepatitis b virus infection and the immune response: The big questions. *Best Practice & Research Clinical Gastroenterology*, 31(3):265–272, 2017.

[4] S. Means, M. A. Ali, H. Ho, and J. Heffernan. Mathematical modeling for hepatitis b virus: Would spatial effects play a role and how to model it? *Frontiers in Physiology*, 11:146, 2020.

[5] I. Widyadharma, P. R. Dewi, I. A. S. Wijayanti, and D. K. I. Utami. Pain related viral infections: A literature review. *The Egyptian Journal of Neurology, Psychiatry and Neurosurgery*, 56(1):1–6, 2020.

[6] S. Schädler and E. Hildt. Hbv life cycle: Entry and morphogenesis. *Viruses*, 1(2):185–209, 2009.

[7] C. Seeger and W. S. Mason. Molecular biology of hepatitis b virus infection. *Virology*, 479: 672–686, 2015.

[8] J. Köck, C. Rösler, J. Zhang, H. B. Blum, M. Nassal, and C. Thoma. Generation of covalently closed circular dna of hepatitis b viruses via intracellular recycling is regulated in a virus specific manner. *PLoS Pathogens*, 6(9):e1001082, 2010.

[9] O. Diekmann and J. A. P. Heesterbeek. *Mathematical Epidemiology of Infectious Diseases: Model Building, Analysis and Interpretation*, volume 5. John Wiley & Sons, 2000.

[10] C. Chiyaka, J. M. Tchuenche, W. Garira, and S. Dube. A mathematical analysis of the effects of control strategies on the transmission dynamics of malaria. *Applied Mathematics and Computation*, 195(2):641–662, 2008.

[11] Z. Mukandavire and W. Garira. Effects of public health educational campaigns and the role of sex workers on the spread of hiv/aids among heterosexuals. *Theoretical Population Biology*, 72(3):346–365, 2007.

[12] M. O. Ogunmodimu, E. P. Enock, A. P. Kenyatta, S. B. Affognon, and F. C. Onwuegbuche. A mathematical model for the prevention of hiv/aids in the presence of undetectable equals untransmittable viral load. *International Journal of Mathematical Sciences and Optimization: Theory and Applications*, 10(2):36–57, 2024.

[13] O. M. Ogunmiloro and A. S. Idowu. Dynamic insights into malaria–onchocerciasis co-disease transmission: Mathematical modeling, basic reproduction number and sensitivity analysis. *Boletín de la Sociedad Matemática Mexicana*, 30(2):27, 2024.

[14] R. A. Mufutau and F. Akinpelu. Sensitivity analysis of mathematical modelling of tuberculosis disease with resistance to drug treatments. *International Journal of Mathematical Sciences and Optimization: Theory and Applications*, 6(2):940–955, 2020.

[15] W. Garira. A complete categorization of multiscale models of infectious disease systems. *Journal of biological dynamics*, 11(1):378–435, 2017.

[16] M. Fallahi-Sichani, M. El-Kebir, S. Marino, D. E. Kirschner, and J. J. Linderman. Multiscale computational modeling reveals a critical role for tnf-α receptor 1 dynamics in tuberculosis granuloma formation. *The Journal of Immunology*, 186(6):3472–3483, 2011.

[17] L. N. Murillo, M. S. Murillo, and A. S. Perelson. Towards multiscale modeling of influenza infection. *Journal of Theoretical Biology*, 332:267–290, 2013.

[18] L. Rong, J. Guedj, H. Dahari, J. Daniel J. Coffield, M. Levi, P. Smith, and A. S. Perelson. Analysis of hepatitis c virus decline during treatment with the protease inhibitor danoprevir using a multiscale model. *PLoS Computational Biology*, 9(3):e1002959, 2013.

[19] B. M. Quintela, J. M. Conway, J. M. Hyman, J Guedj, W. Rodrigo S. Dos, M. Lobosco, and A. S. Perelson. A new age-structured multiscale model of the hepatitis c virus life-cycle during infection and therapy with direct-acting antiviral agents. *Frontiers in Microbiology*, 9:601, 2018.

[20] L. W. Zhang, A. S. Ademiloye, and K. M. Liew. A multiscale cauchy–born meshfree model for deformability of red blood cells parasitized by plasmodium falciparum. *Journal of the Mechanics and Physics of Solids*, 101:268–284, 2017.

[21] F. S. Heldt, T. Frensing, A. Pflugmacher, R. Gröpler, B. Peschel, and U. Reichl. Multiscale modeling of influenza a virus infection supports the development of direct-acting antivirals. *PLoS Computational Biology*, 9(11):e1003372, 2013.

[22] D. Rüdiger, S. Y. Kupke, T. Laske, P. Zmora, and U. Reichl. Multiscale modeling of influenza a virus replication in cell cultures predicts infection dynamics for highly different infection conditions. *PLOS Computational Biology*, 15(2):e1006819, 2019.

[23] W. Garira. A primer on multiscale modelling of infectious disease systems. *Infectious Disease Modelling*, 3:176–191, 2018.

[24] W. Garira. The research and development process for multiscale models of infectious disease systems. *PLoS Computational Biology*, 16(4):e1007734, 2020.

[25] W. Garira. The replication-transmission relativity theory for multiscale modelling of infectious disease systems. *Scientific Reports*, 9(1):1–17, 2019.

[26] J. Nakabayashi. The intracellular dynamics of hepatitis b virus (hbv) replication with reproduced virion "re-cycling". *Journal of Theoretical Biology*, 396:154–162, 2016.

[27] A. Goyal, L. E. Liao, and A. S. Perelson. Within-host mathematical models of hepatitis b virus infection: Past, present, and future. *Current Opinion in Systems Biology*, 18:27–35, 2019.

[28] O. Diekmann, J. A. P. Heesterbeek, and J. A. Metz. On the definition and the computation of the basic reproduction ratio r0 in models for infectious diseases in heterogeneous populations. *Journal of Mathematical Biology*, 28:365–382, 1990.

[29] P. Van den Driessche and J. Watmough. Reproduction numbers and sub-threshold endemic equilibria for compartmental models of disease transmission. *Mathematical Biosciences*, 180 (1-2):29–48, 2002.

[30] C. Castillo-Chavez, S. Blower, P. Van den Driessche, D. Kirschner, and Abdul-Aziz A. Yakubu. *Mathematical Approaches for Emerging and Reemerging Infectious Diseases: Models, Methods, and Theory*, volume 126. Springer Science & Business Media, 2002.

[31] C. Castillo-Chavez and B. Song. Dynamical models of tuberculosis and their applications. *Mathematical Biosciences & Engineering*, 1(2):361–404, 2004.